7

CCDs used in space and at short wavelengths

The current high level of understanding of CCDs in terms of their manufacture, inherent characteristics, instrumental capabilities, and data analysis techniques make these devices desirable for use in spacecraft and satellite observatories and at wavelengths other than the optical. Silicon provides at least some response to photons over the large wavelength range from about 1 to 10 000 Å. Figure 7.1 shows this response by presenting the absorption depth of silicon over an expanded wavelength range. Unless aided in some manner, the intrinsic properties of silicon over the UV and EUV spectral range (1000–3000 Å) are such that the QE of the device at these wavelengths is typically only a few percent or less. This low QE value is due to the fact that for these very short wavelengths, the absorption depth of silicon is near 30–50 Å, far less than the wavelength of the incident light itself. Thus, the majority of the light ($\sim$70%) is reflected with the remaining percentage passing directly through the CCD unhindered.

Observations at wavelengths shorter than about 3000 Å involve additional complexities not encountered with ground-based optical observations. Access to these short wavelengths can only be obtained via space-based telescopes or high altitude rocket and balloon flights. The latter are of short duration from only a few hours up to possibly hundreds of days and use newly developing high-altitude ultra-long duration balloon flight technologies. Space-based observations in the high energy regime from UV to shorter wavelengths usually require detectors to be "solar blind." The term solar blind means that the detector must be completely insensitive to visible light photons. This is generally accomplished by using a non-optically active type of detector or through the use of various types of filters. The majority of astronomical objects emit 10^4–10^6 visible light photons for every UV or shorter wavelength photon; thus even a visible light blocking filter with a 1% visible transmission is not nearly sufficient to remove optical contamination. In addition, most common

https://doi.org/10.1017/CBO9780511807909.009

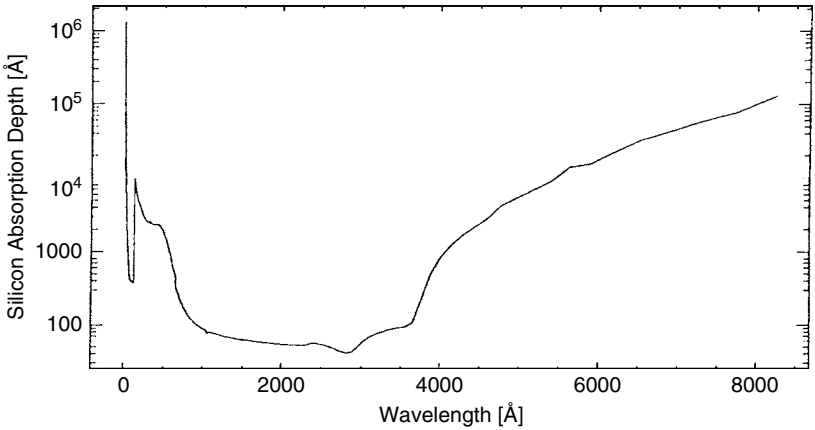

Fig. 7.1. Silicon absorption depth (in Å) from 1.2 to 8500 Å. The vertical axis is a log scale with major tick marks starting at 100 and ending at 10^6. From Bonanno (1995).

filters used to block visible light also absorb some of the incident higher energy radiation as well. Use of such absorbing filters causes even a high QE CCD at UV wavelengths (say 20%) to be reduced to a low effective QE near 2%.

Long-term exposure to high vacuum can cause contamination of the dewar in which the CCD resides. This contamination can be through outgassing of various materials such as vacuum grease or AR coatings (Plucinsky *et al.*, 2004), normally not a problem in well-produced ground-based systems. Exposure to high energy radiation can cause changes in the QE of the CCD or cause permanent damage to the pixels and electronic structures within the array. Studies of the effects of high energy radiation and space environment observations on CCDs are ongoing at a number of laboratories such as the Jet Propulsion Laboratory (for NASA space-based satellites and missions), the Space Telescope Science Institute, and at the European Space Agency (ESA). Good discussions of space-based CCD usage are presented in Janesick, Hynecek, & Blouke, 1981; Janesick, Elliott, & Pool, 1988; Holtzman, 1990; Janesick & Elliott, 1992; Janesick, 2001; Strueder *et al.*, 2002; Meidinger *et al.*, 2004a; Meidinger *et al.*, 2004c, and a number of the websites listed in Appendix B.

Before we discuss the details of observations at wavelengths shorter than the optical, we need to make a brief detour to look into some special issues related to space-based observations with CCDs. The more notable of these issues are the calibration of the CCD throughout the instrument or mission

lifetime, the fact that the point-spread function is much smaller than generally obtained with ground-based data, and continual degradation of the CCD with time as the result of radiation damage.

7.1 CCDs in space

Space-based CCDs have a number of special problems associated with them that are often not considered for ground-based systems. Once launched, human intervention is unlikely and the CCD and instrument package can never be retrieved for fault correction or calibration purposes. Even simple procedures, such as bias calibration, take on new meaning as CCD evolution or changes in the gain or other CCD electronics mean new calibration images are needed. Damage to the array (see Section 7.2), or the possibility that the primary circuits fail and the backup electronics or even a different clocking scheme must be used, means that new calibration images must be produced. Also, each observer does not have the ability to obtain all the needed calibration data and the project must provide the finest and most up-to-date calibration images for each CCD, instrument, and mode of operation. All issues have to be thought out completely prior to launch or dealt with through analysis of downloaded data during the mission.

One such example of a significant change in CCD operation is provided by the Hubble WFPC2 instrument (Holtzman *et al.*, 1995b). After operating in space for only about three months, it was noticed that the CCDs developed an odd sort of CTE effect. The effect caused stars to appear fainter if imaged in higher numbered rows. The apparent cause was the development of a large number of traps within the CCDs not seen during preflight tests. Photometric gradients of 10–15% were present along CCD columns and, even worse, the effect was highly dependent on the brightness of the imaged star, being only about 5% for bright stars.

Using ground-based laboratory tests with similar electronics and CCDs, it was determined that changing the operating temperature from -76°C to -88°C would cause a sharp decrease in the CTE effect. Such a change caused the CTE variations to almost disappear, leaving only a 3–4% gradient. A further temperature decrease would probably improve the situation but in-flight hardware did not allow the CCDs to be operated at colder levels. Thus considerable effort has been put into the development of a semi-empirical software model that can be applied to data obtained with the WFPC2 in order to correct for the remaining effect (Holtzman *et al.*, 1995a; Whitmore & Heyer, 1998). A number of the CCDs in HST instruments and those in the

Chandra X-ray observatory have shown long-term degradation in their CTE performance due to the radiation environment of the telescopes' orbit. For example, the STIS CCDs have changed from a CTE of 0.999 999 to 0.999 91 since launch (Kimble *et al.*, 2000).

One consequence of the CCD operating temperature being lowered in the WFPC2 was decreased dark current. However, on-orbit hot pixel development was greater than expected with many of these hot pixels "fixing" themselves after dewar warming (Section 7.2). Calibration dark frames are therefore required often to monitor the dark current and to provide the best dark frames to use given any set of observational circumstances. Hot pixels are especially important to understand in space-based CCD imagery as the very small PSF of imaged scenes and the appearance of numerous cosmic rays with a plethora of shapes, including single pixel events, must be distinguished from the collected flux of interest.

We alluded above to the importance of cosmic ray identification in order to avoid misinterpretation of imaged scenes. From a sample of 2000-second dark images taken with the WFPC2 it was found that 5–10% of the cosmic ray events were single pixel events of 5 sigma or greater above the bias level. Fully one half or more of these events showed consistent pixel positions from frame to frame and thus could not be identified with true cosmic rays or local radioactivity from the dewar and surroundings. Typical signal levels for true single pixel cosmic ray events were near 200 electrons while multiple events peaked near 700 electrons (Holtzman *et al.*, 1995b). Multiple pixel cosmic ray hits (averaging seven affected pixels per event) are much more common than single pixel events, and a rate of almost two events per CCD per second was observed.

CCD dewars, once sealed, evacuated, and chilled, are often seen to produce contaminants owing to outgassing of grease or other coatings used in their construction. When at operating temperatures of $-80°$ C or so, the dewar window is a good site for condensation of such contaminants. These small particles of material are very good absorbers of light, particularly UV and visible radiation, because of their characteristic sizes. A likely cause of the contamination is C, O, and F atoms that often form a thin layer on the dewar window or instrument filters quickly and then increase this layer slowly with time. Bake-out procedures have been modeled as a possible method to reduce the thickness of these layers (Plucinsky *et al.*, 2004) specific to the ACIS CCDs on the Chandra X-ray observatory.

One simple calibration test that allows monitoring of this effect is to obtain fairly regular observations of a bright UV star. If the dewar window does indeed get fogged with material, careful measurements of the UV throughput

of the observed flux will show a slow degradation. Even in the best space-based instruments, small amounts of material outgas, and after several weeks UV performance can be noticeably lower. One solution that seems to work, at least for the Hubble Space Telescope WFPC2 CCDs and the Chandra X-ray observatory ACIS CCD imager (and for general observatory dewars), is to warm the dewar up to allow for thermal desorption. The WFPC2 CCDs were warmed to near 20° C for about 6 hours approximately every month. In a typical observatory dewar after warm up, one can attach a vacuum pump and pump out the now non-frozen water and other contaminants, then recool the device.

Flat fields, as we have discussed before, are very important to have in one's calibration toolkit. Once in orbit, either as a satellite or as a spacecraft destined for another world, the CCDs aboard generally have little ability to obtain flat field calibration images. High S/N flats made prior to launch in the laboratory are often the best available. These usually provide overall correction to 5% or a bit better, but small effects, such as illumination or instrument changes, limit the accuracy of the correction. Sometimes, the space-based CCD has significant changes, and large corrections are needed or new flats have to be generated in some manner.

The original WFPC camera aboard Hubble could obtain on-orbit flats through observation of the bright earth (Holtzman, 1990; Faber & Westphal, 1991). These were not elegant flats, having streaks and nonuniformities, but were all that was available. WFPC2 used Loral CCDs, which have an increased stability over the original TI CCDs, allowing preflight laboratory flats to work very well, even after the reduction in operating temperature as discussed above. Numerous other small effects, such as color dependence, radiation damage, hot pixels, CCD illumination, and optical distortions seen in the on-orbit WFPC2 flats are discussed in detail in Holtzman *et al.* (1995b). The effects of flat fielding, CTE, and the other issues discussed above on the photometric performance of the Hubble WFPC2 are described in Faber & Westphal (1991), Holtzman *et al.* (1995a), and Whitmore & Heyer (1998).

The Galileo spacecraft certainly provided impressive imagery of the planet Jupiter and its satellites and was one of the first public CCD cameras to be launched into space. Its CCD camera is described in detail in Belton *et al.* (1992) and can be used as an example of the details of space-based observations, their calibrations, properties, and difficulties. CCD and instrument stability and processes for their calibration after launch are major effects to consider as well as proper treatment of the photometric calibration images in lieu of the much reduced PSF.

The solid-state imager (SSI) aboard Galileo consisted of a single 800×800 TI CCD with a read noise of 40 electrons, gains of 38 to 380 electrons per DN, and a pixel size of 15 microns yielding 2.1 arcsec per pixel. The SSI, like the WFPC2, developed a CTE problem after about 8–12 months in space. Detailed study of SSI images taken during periods of cruise science (Howell & Merline, 1991) revealed that the CTE problem resulted in a readout tail containing 400 electrons, independent of the brightness of an imaged star or its location within the CCD. The cause was attributed to a trap, not in the active CCD array, but in the output register. Radiation damage (see next section) was the most likely cause. Due to the constant number of trapped electrons, photometric correction was possible to a high degree of accuracy.

Point sources imaged in space are free from the blurring effects of the Earth's atmosphere and have a very small PSF compared with those commonly obtained with ground-based telescopes. A theoretical diffraction-limited image formed through a circular open aperture will have a FWHM (of the Airy disk) in radians of

$$\mathrm{FWHM} = \frac{1.03\lambda}{D},$$

where λ is the wavelength of observation and D is the diameter of the aperture (Born & Wolf, 1959). Note that if we were to use the radius of the first Airy disk dark ring as our definition of image size, we would have the traditional formula

$$r = \frac{1.22\lambda}{D}.$$

Figure 7.2 shows theoretical Airy disk PSFs expected to be imaged by the SSI at three representative wavelengths and five different possible slight de-focus values.

The FWHM of the SSI images (being obtained without any atmospheric or other seeing effects) were predicted to be about 0.55 arcsec at 4000 Å and 1.2 arcsec at 9000 Å. These PSF sizes correspond to 0.25 and 0.6 pixels respectively, making the SSI images severely undersampled ($r \sim 0.2$). This level of undersampling makes it impossible to directly determine the true FWHM or profile shape of a PSF. Using multiple images with slight offsets, images containing multiple stars with different pixel grid placements, and model CCD images, one can reconstruct the true PSF imaged by an undersampled space-based CCD camera. In the SSI case, the PSF was found to be slightly larger than predicted and attributed to a slight camera focus problem.

As we have seen, undersampled images will lead to astrometric and photometric error, as the lack of a well-sampled PSF makes it hard to determine the true image center or the actual flux contained in the image. For the SSI,

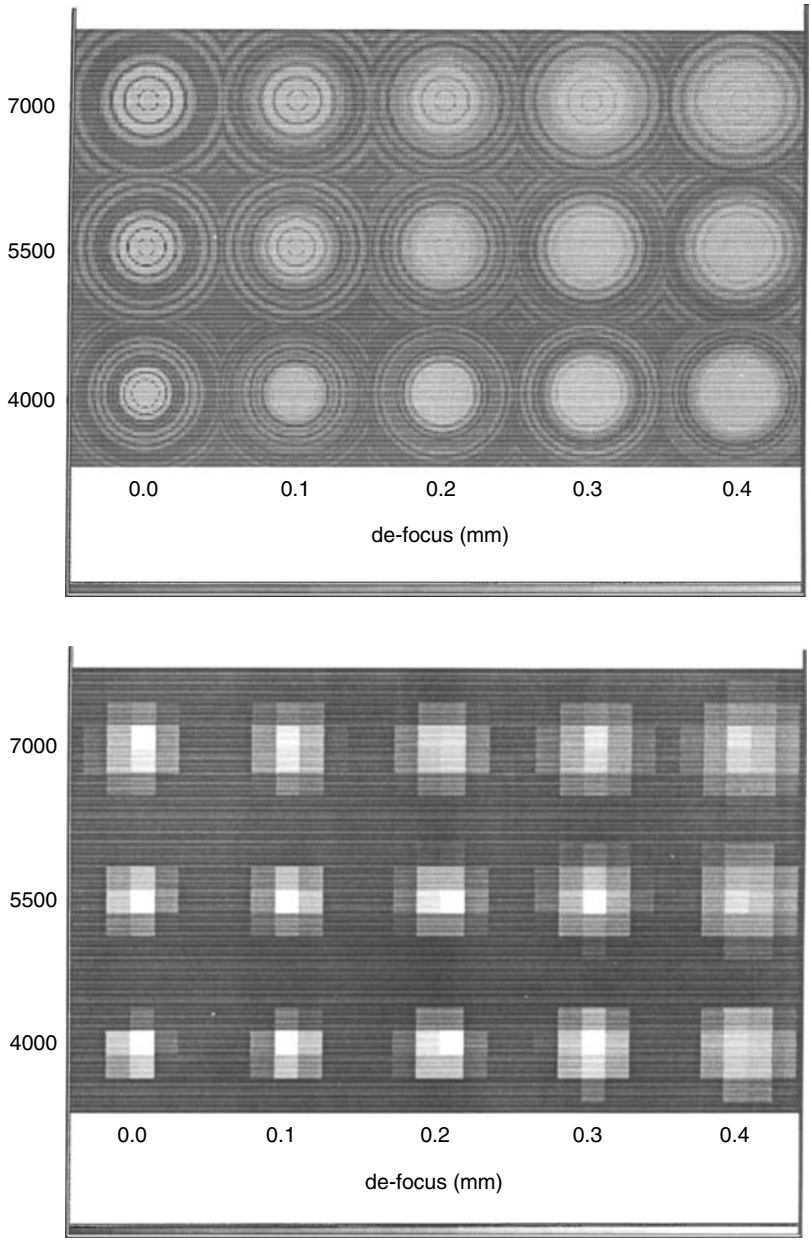

Fig. 7.2. Modeled Airy disk patterns imaged by the Galileo SSI. The top panel shows the calculated PSFs as would be seen under very well-sampled conditions while the bottom panel shows the same PSFs as they would appear when imaged by the SSI. The severe pixelization of the PSFs is apparent. The rows are for 7000, 5500, and 4000 Å (top to bottom) and the five columns are (left to right) de-focus values for the SSI camera in mm. From Howell & Merline (1991).

astrometric error amounted to about 0.8 arcsec even for bright stars, or about half a pixel. Observations of bright guide stars are a common occurrence for spacecraft and are used for navigation and course correction. Large astrometric uncertainties are hazardous and can lead to spacecraft orbital trajectories with inaccurate pointings, having the potential of producing spacecraft course corrections that could cause it to miss a target or, even worse, come too close. In the Galileo case, it was determined that a large number of guide star images was needed and careful analysis of these could be used to determine the path and navigation of the spacecraft within acceptable limits.

Photometrically, the nature of the undersampling manifests itself in two ways. First is the way in which one extracts the data and how a flux value is assigned to it; second is the effect of digitization noise, which is large for the SSI. Figure 7.3 illustrates the first of these issues by presenting SSI data for a bright star. Because of the nature of the PSFs imaged with the SSI,

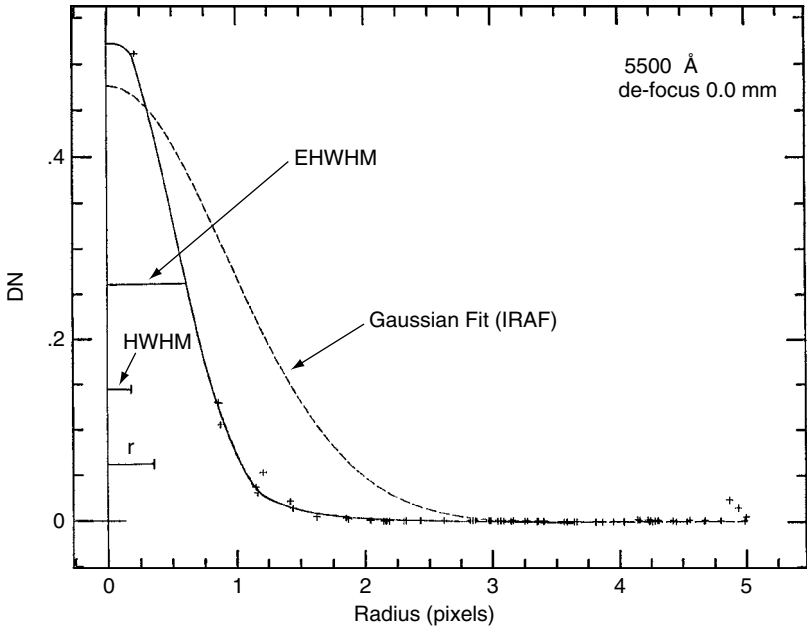

Fig. 7.3. Radial profile plot of a bright star imaged by the Galileo SSI. The plus signs are the actual CCD DN values (for $G = 380\,e^-/DN$) and HWHM and r correspond to predicted values for an Airy disk imaged at 5500 Å. Note that an approximation as a Gaussian profile is a poor representation of the actual PSF but the determined EHWHM for a single measurement is not far off. From Howell & Merline (1991).

one pixel (plus sign at $r = 0.25$) contains much more flux than any of the remaining ones. A standard Gaussian fit to these data (in this case made by IRAF) is seen to provide a complete misrepresentation of the image profile. Imagine the photometric error one would introduce by assumption of this type of profile and use of its shape as an indication of the total counts observed for this star. The effective FWHM (EFWHM) is defined as the apparent PSF width as determinable from a single undersampled image of a star. We see here that the EHWHM is 0.7 pixels, compared with the expected value (at 5500 Å) of 0.55. The digitization effect present at the highest SSI gain setting leads to an uncertainty of ±379 electrons per DN. The above effects combined lead to an overall relative photometric uncertainty of 5–10% and an absolute spectrophotometric uncertainty of 10–30% for SSI data. These are higher than the 2–5% uncertainties quoted for the WFPC2 camera and are directly in proportion to the greater undersampling and higher CCD gain values used in the Galileo SSI.

Further readings concerning the special conditions and circumstances of CCDs when used for space-based observations can be found with a quick search of the websites of the Hubble Space Telescope and other satellite and spacecraft observatories. Access to numerous internal technical, engineering, and calibration reports is given as well as literature articles containing applications of the findings to astrophysical objects.

7.2 Radiation damage in CCDs

With the launch of the Galileo spacecraft and the Hubble Space Telescope, astronomical imagery with CCDs from outer space began. Today Cassini, Deep Impact, Chandra, XMM-Newton, and a number of other satellitees and space missions (such as the proposed Constellation-X, DUO, ROSITA, and GAIA space missions) have CCD imagers on-board. With these exciting new windows on the Universe come many unexpected effects in the performance and output noise levels of the CCDs involved. The study of radiation damage in CCDs had occurred in a number of military projects, but the low incident flux and low noise levels needed for astronomy required new laboratory work and the development of techniques to deal with or avoid radiation effects altogether (Cameron *et al.*, 2004; Meidinger *et al.*, 2004a; Meidinger *et al.*, 2004b).

The hostile conditions expected in outer space were not the only radiation source to be concerned about for CCDs. Satellites in low Earth orbit, such as the Hubble Space Telescope, pass through the South Atlantic Anomaly

(SAA) periodically, receiving a healthy dose of high energy protons. The Chandra X-ray observatory's largest factor that reduces observing efficiency is the interruption of observations due to passage through the Earth's radiation belts every 2.6 days. X-ray observations are suspended for ~15 hours and the X-ray imager is purposely defocused to minimize damage from low energy (100–200 keV) protons (DePasquale *et al.*, 2004). Solar satellites, such as CAST, are also prone to harsh radiation environments (Kuster *et al.*, 2004). Deep space missions like Galileo and Cassini have a radioisotope thermal electric generator (RTG) to provide power for the spacecraft as well as a neutron dose that bathes the on-board CCD imager. These inherent radiation environments, along with the general space background of cosmic rays and high energy particles from such events as solar flares or planetary magnetic fields, cause both temporary and permanent damage to a CCD in addition to long-term degradation.

Ironically, as CCDs became better astronomical devices in terms of their low read noise and dark currents, they also became much more susceptible to damage by high energy radiation. The SAA, for example, provides about 2000 protons per square centimeter per second with energy of 50–100 MeV, for each passage. Galileo's RTG produced 10^{10} neutrons per square centimeter at the location of the CCD over the expected six-year mission lifetime. Passage through Jupiter's radiation belts near the moon Io was predicted to provide a 2500 rad dose of radiation to the CCD with each orbit. These levels of radiation do indeed cause damage to the CCD involved and methods of monitoring the changes that occur with time and the development of new manufacturing techniques aimed at radiation hardness were needed (McGrath, 1981).

The two major areas of concern in radiation damage to CCDs are (1) high energy photon interactions, which result in fast electrons, which in turn cause simple, localized damage defects and the generation of numerous electron–hole pairs, and (2) nuclear reactions caused by uncharged neutrons or high energy protons, which cause large area defects and are more likely to lead to partial or complete failure of a device (Janesick, Elliott, & Pool, 1988; Janesick, 2001). The first of these radiation induced concerns is called an ionization effect and involves gamma rays or charged particles. The second, involving massive particles, is termed a bulk effect or displacement damage owing to its ability to displace silicon atoms from their lattice positions within the CCD.

Displacement damage can involve single silicon atoms or bulk damage involving clusters of atoms, all removed from their original lattice locations within the CCD. The vacancies remaining in the lattice structure create trapping locations, which in turn cause degraded or no CTE performance for one

or more pixels in the array. As the result of lattice stresses, the trap locations become populated by one or more of the doping elements such as phosphorus. The presence of a phosphorus atom within the silicon lattice modifies the band gap energies locally and is thought to be the cause of observed reduced CTE effects (Srour, Hartmann, & Kitazaki, 1986). The CTI performance of the front illuminated CCDs aboard HST suffered radiation damage from exposure to soft protons when passing through the SAA. The damage increased the CTI by more than two orders of magnitude (Grant *et al.*, 2004) and the observatory team has developed a model of the damage to help mitigate its effect on observations.

Repair of some percentage of single lattice displacement defects (i.e., hot pixels) has been accomplished by cycling the CCD to room temperature or higher and back again to operating temperature, a process called annealing. The back-side, thinned SITe CCDs in the HST Advanced Camera for Surveys (ACS) undergo a routine monthly annealing process. Hot pixels (pixels with enhanced dark current of 0.04 electrons/pixel/s or more), appear at a rate of $\sim$1230 per day in the ACS CCDs. Annealing the detectors will fix about 60–80% of new hot pixels (new since the last anneal) but very few of the older hot pixels are repaired. Figure 7.4 illustrates this procedure for the ACS Wide Field Camera (WFC) CCDs in the ACS.

Bulk defects in CCDs are essentially impossible to repair. It has been noticed, however, that at low temperatures ($< -100^{\circ}$ C), the trapped charge

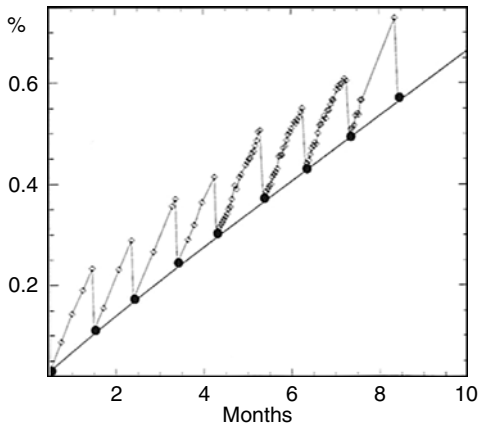

Fig. 7.4. This figure shows the growth in the number of ACS/WFC hot pixels since installation aboard the HST. One can see the lowering of the hot pixel count through monthly anneals as well as the continued overall evolution to increasing numbers. From Clampin *et al.*, 2002.

accumulated at the defect location remains trapped and has little effect on the overall CTE. This temperature dependence has been shown to be proportional to $\exp(-E_T/kT)$, where E_T is the activation energy of the lattice traps (Janesick, Elliott, & Pool, 1988). Thus one way to avoid lattice defects is to operate the CCD at temperatures as low as possible. Interestingly, high temperature operation ($>30°$ C) allows trapped charge to be released very quickly, eliminating a deferred charge tail and providing good CTE. These various techniques involving temperature manipulation of a CCD system are often hard to employ practically in space. Additionally, the temporal behavior of the CCD involved can be unpredictable and may be different for each CCD, even those of the same type.

Ionization effects, caused by gamma rays or charged particles, cause a charge buildup in the CCD gate structures and can produce increases in the CCD dark current. Whereas a 150 keV electron is needed to cause an actual silicon atom displacement, only a few eV of energy deposited in the gate insulator is enough to change the potential and cause charge trapping. Even an intense UV flood (Ditsler, 1990; Schaeffer *et al.*, 1990) with 2500 Å photons can cause dark current increases or even render the CCD inoperable. The charge buildup causes new states to exist within the band gap of the silicon leading to easier generation of thermal electrons and thereby an increased dark current. The affected CCD pixels, that is, those that have been damaged by the ionizing radiation, will show increased dark current, while their neighbors will not. Histograms of the amount of dark current produced as a function of pixel signal level often show "spikes" of dark current at specific signal levels. This is taken to indicate a sort of quantized structure in the amount of damage that occurs per radiation site (Janesick, Elliott, & Pool, 1988).

Additional damage to CCDs in space by micrometeoroids has recently been studied (Meidinger *et al.*, 2003) for the CCDs on the XMM-Newton X-ray satellite. Other background increasing radiation events occur as well (Freyberg *et al.*, 2004; Katayama *et al.*, 2004) even if their cause remains a mystery.

Methods of protecting CCDs from radiation effects are varied. The type and amount of radiation expected and the scientific goals of the imager must be carefully weighed to produce the final compromise. For example, the CCD flown on the Galileo mission was initially tested for its ability to withstand gamma radiation similar to that expected in the Jovian magnetic fields, a test that it passed well. It was probably by shear luck that a test or two was also performed to understand its performance when exposed to neutrons. Neutron bombardment revealed an increased dark current was prevalent in the CCDs and a redesign of the imager was needed. To mitigate the problem,

the CCD imager had its operating temperature changed to −130° C compared with the original specified value of −40° C. In the case of the Hubble Space Telescope CCDs, increased dark current is not a large factor because of their colder operating temperature, but long-term degrading CTE and QE effects have been seen (Holtzman, 1990; Clampin *et al.*, 2002) and attributed to in-orbit radiation damage. A detailed report of the detectors in the Hubble telescope is contained in Brown (1993) and considerations on improving the ability of CCDs to counteract the effects of radiation are discussed in IEEE Nuclear Science Symposium (1988), Bely, Burrows, & Illingworth (1989), and Janesick (2001).

7.3 CCDs in the UV and EUV (300–3000 Å) spectral range

Progress in the use of CCDs for UV and EUV observations has occurred on two main fronts. Coatings applied to the CCDs to down-convert high energy photons to visible light photons is one method. The other method involves new manufacturing techniques that allow short wavelength photons to penetrate the silicon even given the very small absorption depths at these wavelengths.

Coating the CCD with a UV phosphor has been discussed previously in this book (Chapter 2) with regard to enhancement of the near-UV wavelength range. These same coatings can often increase the QE of a CCD to usable levels, down to wavelengths as short as 500 Å. Lumogen, a UV phosphor that absorbs photons of $\lambda < 4200$ Å and reemits their energy near 5200 Å, is a popular choice. This inexpensive material is thermally deposited onto the CCD surface while under vacuum into a layer about 6000 Å thick. Use of lumogen as a coating delivers a QE from 500–4000 Å of around 15% (yielding about 3% with a solar blind filter in place) and actually increases the intrinsic QE from 5000 to 8000 Å, as it acts as an antireflection coating. Phosphor coatings can be deposited onto either front- or back-side illuminated CCDs (McLean, 1997c; Lesser, 2002). Other coatings such as coronene and Metachrome II are also used for UV and EUV enhancement (Geary *et al.*, 1990; Schempp, 1990; Trauger, 1990).

Modern manufacturing processes have again come to the rescue through the development of techniques that allow the CCD itself to have more sensitivity to short wavelength photons. We have mentioned before that the gate structures of a CCD can absorb short wavelength photons before they enter the actual pixel itself, thus reducing or eliminating the collection probability at these wavelengths. Solutions to this problem consisted of using a back-side

illuminated, thinned device or making CCDs with transparent gates. Both of these techniques can be further improved and employed for detection of UV and shorter wavelength photons.

During the thinning process, the back-side of a CCD forms an oxide layer, which can include a surface layer of incomplete bonds that are positively charged. With the very short absorption depths for UV and shorter wavelength photons, any photoelectrons produced within the silicon are more likely to be attracted to the positive bonds where recombination occurs, and not to the pixel potential well for collection, storage, and output. Various techniques have been developed to reduce the number of positive incomplete bond sites that exist in a thinned CCD (Janesick *et al.*, 1985; Janesick *et al.*, 1989; Baily *et al.*, 1990). Additionally, methods that allow removal of the oxide layer produced in the thinning process have been developed and consist of precision etching of the oxide layer under controlled conditions (Bonanno, 1995).

Recent detailed work, aimed at understanding the characteristics and performance of CCDs in the wavelength range of 300–4000 Å, has been performed. The laboratory setup used and various types of short wavelength enhanced CCDs produced and tested are described in Bonanno (1995), which concludes that QE values of 10–60% can be achieved over the wavelength range of 300–2500 Å. These same CCDs also have up to 80% QE at 6000 Å. Phosphor coatings and manufacturing improvements are about equal in their ability to enhance UV and EUV performance; however, both types of improvement appear to show a decrease in their QE with time, once the CCD is cooled and put under vacuum. Contamination by outgassing within the vacuum and subsequent freezing of the contaminants onto the CCD surface are thought to be the most likely causes of the reduced QE.

To overcome the low QE of CCDs at short wavelengths, even after the above enhancements have been performed, some high-energy applications employ standard unmodified CCDs as detectors, preceded in the optical path by a device such as a microchannel plate (MCP). MCPs can produce up to about 500 000 electrons per incident high energy photon, and this electron cloud strikes a phosphor coated photocathode producing visible light photons that are collected and imaged by the CCD (Eccles, Sim, & Tritton, 1983). MCPs operate at high voltages (a few keV) and are inherently solar blind as they require high energy photons for activation. Final QE values of up to 20% are possible with a well-constructed device. This increased QE is the largest advantage of instruments that use intensified CCDs, while poor spatial resolution, phosphor decay effects, and smaller dynamic range (compared with a normal CCD) are the major disadvantages (McLean, 1997c; Longair, 1997).

https://doi.org/10.1017/CBO9780511807909.009

7.4 CCDs in the X-ray (<500 Å) spectral range

Figure 7.1 provided hints that CCDs may also be useful detectors for the X-ray region of the spectrum, as the absorption depth within silicon rises shortward of about 1000 Å. Figure 7.5 shows us a similar result, only this time we express it as the quantum efficiency of the CCD as a function of photon energy or wavelength. We note that within the X-ray region, back-side thinned CCDs are extremely efficient detectors, approaching a quantum efficiency of 100% at times. The X-ray telescopes aboard XMM-Newton and Chandra use CCDs as their detectors (Longair, 1997; Marshall *et al.*, 2004; Sembay *et al.*, 2004).

X-ray detection by CCDs works in a slightly different manner from detection of optical photons. An incident optical photon creates a photoelectron within the silicon lattice, which moves from the valance to the conduction band and is then held there (in a pixel) by an applied potential. The absorption of an X-ray photon by silicon ejects a free, fast moving, photoelectron of energy $E - b$, where $E = h\nu$ and b is the binding energy of the electron to the silicon atom, typically 1780 eV. As this highly energetic electron moves through the silicon lattice, it produces a trail of electron–hole (e–h) pairs,

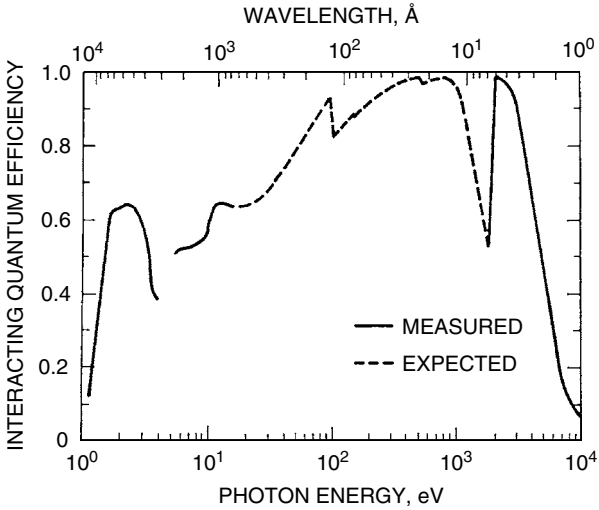

Fig. 7.5. Quantum efficiency for a typical thinned, back-side illuminated CCD from the X-ray to the optical spectral regions. From Janesick *et al.* (1988).

with each requiring an average of 3.65 eV of energy to be produced.[1] Each incident X-ray photon collected produces a measureable number of e–h pairs, thus yielding a method by which one can backtrack and obtain the incident photon energy (Longair, 1997). If all the energy of the free electron went into the e–h pair production, the energy of the incident X-ray could be precisely knowable simply by counting the ADUs produced within the CCD pixels. This property leads to an interesting aspect of X-ray imaging in that one can use the number of photoelectrons produced by an incoming photon to tell its incident energy (wavelength), thereby performing imaging and (crude) X-ray spectroscopy simultaneously.

However, a small undetermined amount of the free electron's energy goes into various phononic states of the silicon lattice, thereby causing some uncertainty in the value of the incident photon's energy. The level of this uncertainty, the "Fano" factor,[2] is so small that to obtain Fano-noise limited CCD performance, the CCD read noise must be less than about 2 electrons (Janesick *et al.*, 1988; Janesick, 2001). Imaging an ^{55}Fe source (used to measure CTE – Chapter 3), would produce a single spectral line at the 5.9 keV Fe Kα energy level while imaging a real astronomical source would produce a crude X-ray spectrum covering the energy range of the detected photons. This type of X-ray spectroscopy was used to produce very low resolution spectra using the imaging capabilities of the ROSAT X-ray satellite.

The Chandra telescope obtains X-ray images and spectroscopy but, in this case, the spectra are not produced by unfolding the images via monitoring image energy deposition, but through the use of gratings to disperse the X-rays (Marshall *et al.*, 2004) in the same manner as discussed for optical spectroscopy in Chapter 6. The imaging and spectroscopy on Chandra both use MIT/LL CCD detectors. These devices are 1024×1024 frame transfer CCDs with 24 micron pixels. The frame transfer nature of the CCDs provides fast readout capabilities and therefore can act as an electronic shutter for X-ray observations. Some of the CCDs are front-side illuminated CCDs but these have suffered a lot of damage from the X-rays incident on their (front-side) gate structures (Grant *et al.*, 2004). The back-side illuminated CCDs fare better in terms of radiation damage as well as having overall better QE at lower energy (Figure 7.6).

Figure 7.7 shows an X-ray spectrum of the star Capella obtained with the Chandra observatory using the high energy transmission grating (HETG).

[1] Note this value is about equal to the energy of a typical optical photon, which we already know produces one photoelectron.

[2] The term Fano factor is due to U. Fano who, in 1947, formulated a description of the uncertainty in the energy of ion pairs produced in a gas by ionizing radiation.

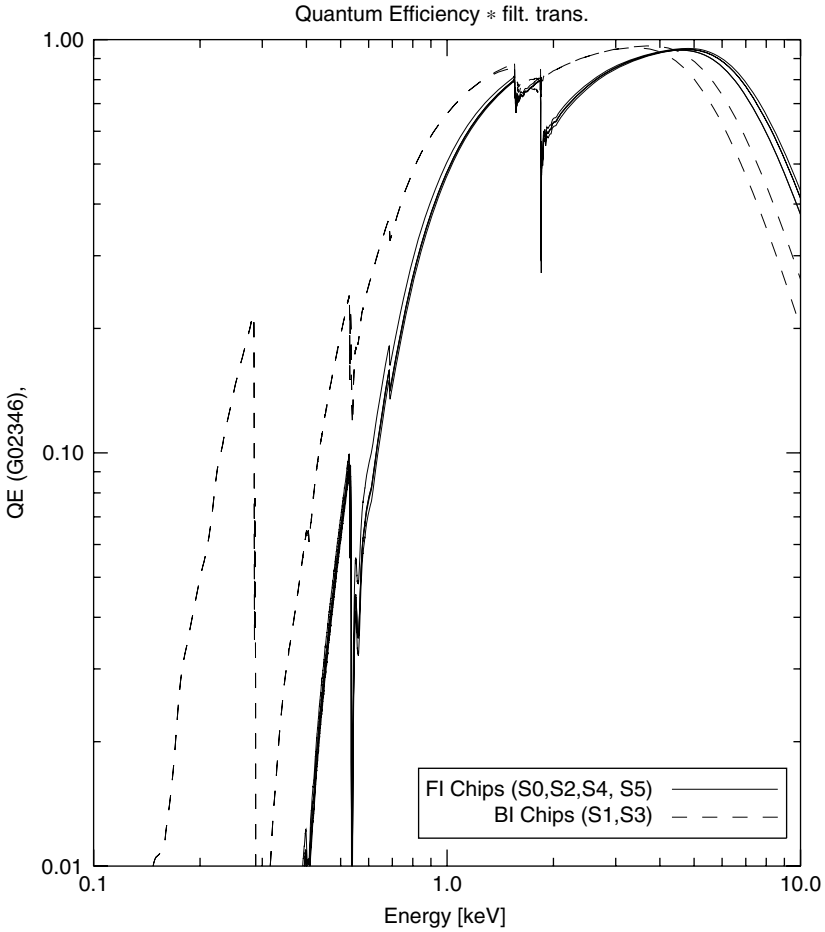

Fig. 7.6. X-ray QE for the CCDs aboard the Chandra X-ray observatory. These QE curves are those of the CCDs convolved with the X-ray filters used. The QE jumps or "edges" seen are caused by inner electronic shell energies of the elements, such as C, used in the X-ray filters.

The spectrum covers the wavelength range from 6–18 Å and shows emission lines (identified in the figure) due to the hot (1 million kelvins or more) stellar corona. XMM-Newton, another X-ray satellite currently in operation, also uses CCDs as detectors. Both of these orbiting X-ray observatories have detailed web pages discussing their telescopes and detectors. A full description is beyond the scope of this volume, but Appendix A contains a number of interesting links to explore.

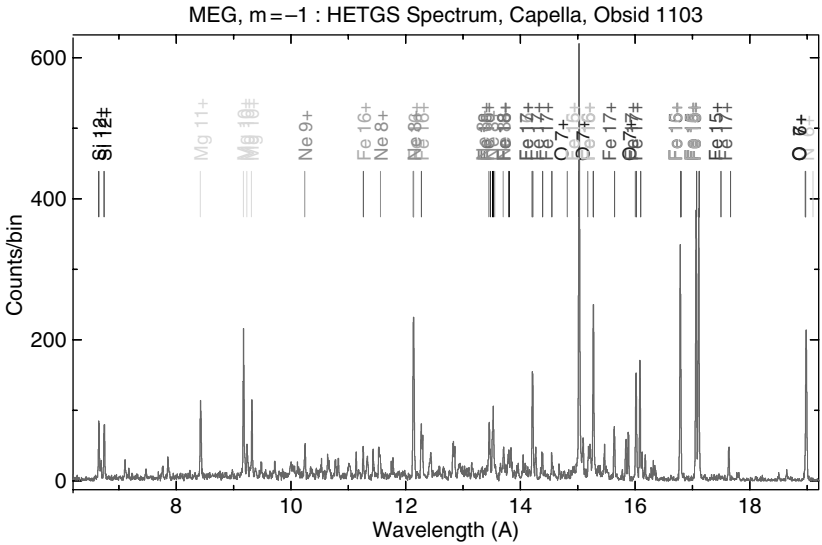

Fig. 7.7. X-ray spectrum of the star Capella obtained with CCDs aboard the Chandra X-ray observatory. The strong emission lines are produced in the hot corona of the star.

7.5 Exercises

1. Make a list of astronomical sources that have their largest flux output at each of the following wavelengths: X-ray, UV, optical, IR, and radio.
2. Which wavelengths require space-based observations?
3. Why do cosmic rays in ground-based CCD images generally produce single pixel events while those in space-based CCD images can produce long streaks and wiggles, as well as single pixel events?
4. Which type of radiation damage has a greater effect on photometric observations from space? Which type affects spectroscopic observations more?
5. Using the idea of charge diffusion and applying it to silicon atoms in a CCD lattice, can you provide a quantitative description of how annealing a CCD "fixes" the majority of hot pixels?
6. Produce a list of items that are required to be different for a CCD camera operating in Earth orbit compared with a similar camera used at a ground-based telescope. Pay particular attention to the plate scale and the A/D process.

7. Describe an observational program that would allow photometric calibration of a CCD camera aboard an interplanetary spacecraft. What level of accuracy would you expect to achieve?
8. Using the locations of the edges in the QE plot for the CCDs (Fig. 7.6), determine which elements and which K shell electron transition is responsible for each.
9. For a CCD used at X-ray wavelengths, describe in detail the procedure that would allow an X-ray image to produce a low resolution spectrum of the imaged source. Convert the x-axis of the X-ray spectrum shown in Figure 7.7 into keV. Make a plot of the relationship between wavelength and number of generated photoelectrons produced for a given X-ray photon in the spectrum.